Chapter 8

Spatial $\mathcal{H}_\infty$ control

In this chapter, we will describe a controller design framework for structural vibration control that is based on the spatial $\mathcal{H}_\infty$ norm concept. The concept was originally introduced in [MPP97]. We use the concept to design a spatial $\mathcal{H}_\infty$ controller for vibration control of smart structures. In particular, we implement the controller on a piezoelectric laminate beam to demonstrate its effectiveness in minimizing structural vibration [HM01b, HM02a]. The controller is designed to minimize the spatial $\mathcal{H}_\infty$ norm of the closed-loop system. Minimizing the spatial $\mathcal{H}_\infty$ norm of the system will ensure vibration suppression over the entire structure in a spatially-averaged sense.

8.1 Spatial $\mathcal{H}_\infty$ control of flexible structures

Consider a typical disturbance rejection problem for flexible structures as in Figure 7.1. The spatial $\mathcal{H}_\infty$ controller is developed to reduce the effect of disturbance w on the entire structure.

A spatially distributed LTI dynamical system is again defined as:

$$\begin{aligned} \dot{\bar{x}}(t) &= A\bar{x}(t) + B_1 w(t) + B_2 u(t) \\ y(t,r) &= C_1(r)\bar{x}(t) + D_{11}(r)w(t) + D_{12}(r)u(t) \\ V_s(t) &= C_2\bar{x}(t) + D_{21}w(t) + D_{22}u(t) \end{aligned} \tag{8.1}$$

where all parameters are defined in (7.1).

The spatial $\mathcal{H}_\infty$ control problem is to design a controller

$$\begin{aligned} \dot{x}_k(t) &= A_k x_k(t) + B_k V_s(t) \\ u(t) &= C_k x_k(t) + D_k V_s(t) \end{aligned} \tag{8.2}$$

such that the closed-loop system satisfies

$$\inf_{K \in U} \sup_{w \in \mathcal{L}_2[0,\infty)} J_\infty < \gamma^2 \tag{8.3}$$

where U is the set of all stabilizing controllers and

$$J_\infty = \frac{\int_0^\infty \int_{\mathcal{R}} y(t,r)^T Q(r) y(t,r) dr dt}{\int_0^\infty w(t)^T w(t) dt} \tag{8.4}$$

where $Q(r)$ is a spatial weighting function and $r \in \mathcal{R}$.

The numerator in (8.4) is the weighted spatial $\mathcal{H}_2$ norm of signal y as in Definition 3.3. Therefore, J_∞ can be interpreted as the ratio of the spatial energy of the system output to the energy of its input. The control problem is depicted in Figure 8.1.

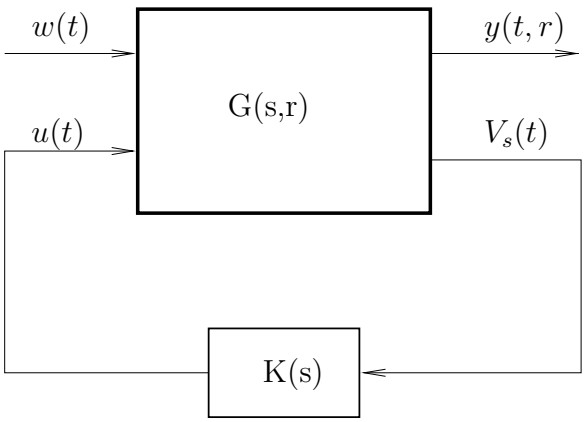

Figure 8.1: Spatial $\mathcal{H}_\infty$ control problem

We can solve the spatial $\mathcal{H}_\infty$ control problem by noticing that it is equivalent to a standard $\mathcal{H}_\infty$ control problem with

$$J_\infty = \frac{\int_0^\infty \tilde{y}(t)^T \tilde{y}(t) dt}{\int_0^\infty w(t)^T w(t) dt}. \tag{8.5}$$

The representation in (8.5) can be obtained by representing y in (8.1) as:

$$y(t) = [C_1(r) \;\; D_{11}(r) \;\; D_{12}(r)] \begin{bmatrix} \bar{x} \\ w \\ u \end{bmatrix}. \tag{8.6}$$

Hence, it can be shown that

$$\begin{aligned} \tilde{y}(t)^T \tilde{y}(t) &= \int_{\mathcal{R}} y(t,r)^T Q(r)\, y(t,r) dr \\ &= \begin{bmatrix} \bar{x}^T & w^T & u^T \end{bmatrix} \Gamma^T \Gamma \begin{bmatrix} \bar{x} \\ w \\ u \end{bmatrix} \end{aligned} \tag{8.7}$$

where Γ is a matrix that satisfies

$$\Gamma^T \Gamma = \int_{\mathcal{R}} \begin{bmatrix} C_1(r)^T \\ D_{11}(r)^T \\ D_{12}(r)^T \end{bmatrix} Q(r) \; [C_1(r) \quad D_{11}(r) \quad D_{12}(r)] \; dr. \tag{8.8}$$

The above problem is then equivalent to a standard $\mathcal{H}_\infty$ control problem for the following system:

$$\begin{aligned} \dot{\bar{x}}(t) &= A\bar{x}(t) + B_1 w(t) + B_2 u(t) \\ \tilde{y}(t) &= \Pi\, \bar{x}(t) + \Theta_1 w(t) + \Theta_2 u(t) \\ V_s(t) &= C_2 \bar{x}(t) + D_{21} w(t) + D_{22} u(t) \end{aligned} \tag{8.9}$$

where $[\Pi \quad \Theta_1 \quad \Theta_2] = \Gamma$. If the disturbance w is assumed to enter through the actuators as shown in Figure 7.1, then $D_{21} = D_{22}, D_{11}(r) = D_{12}(r)$ and $B_1 = B_2$.

The system in (8.9) can be solved using a standard $\mathcal{H}_\infty$ control technique [ZDG96, PAJ91]. The $\mathcal{H}_\infty$ control problem associated with the system described in (8.9) is non-singular. The non-singular system is obtained because of the existence of feedthrough terms from the disturbance to the measured output and from the control signal to the performance output. Therefore, the advantage

of adding feedthrough terms to correct the model is two-fold. Without the feedthrough terms, the resulting $\mathcal{H}_\infty$ control problem would be singular.

Similar to the case of spatial $\mathcal{H}_2$ control, a weight on the control signal may be required to avoid excessive controller gain. It should be noted that the term Θ_2 in (8.9) does not represent a physical weight on the control signal since it represents the effect of truncated modes on the in-bandwidth dynamics of the system. Thus, the system (8.9) can be modified by introducing a weight on the control signal:

$$\begin{aligned} \dot{\bar{x}}(t) &= A\bar{x}(t) + B_1 w(t) + B_2 u(t) \\ \hat{y}(t) &= \begin{bmatrix} \Pi \\ 0 \end{bmatrix} \bar{x}(t) + \begin{bmatrix} \Theta_1 \\ 0 \end{bmatrix} w(t) + \begin{bmatrix} \Theta_2 \\ R \end{bmatrix} u(t) \\ V_s(t) &= C_2 \bar{x}(t) + D_{21} w(t) + D_{22} u(t) \end{aligned} \tag{8.10}$$

where R is a weighting matrix with compatible dimensions.

Therefore there is a compromise between the controller effort with respect to the degree of vibration reduction that can be achieved. Adding this control weight can be shown to be equivalent to adding a term $\int_0^\infty u(t)^T R^T R u(t) dt$ to the numerator of the cost function J_∞ in (8.4).

8.2 Spatial $\mathcal{H}_\infty$ control of a piezoelectric laminate beam

We will design and implement the spatial $\mathcal{H}_\infty$ control method to minimize vibration of a piezoelectric laminate beam. The piezoelectric laminate beam in Chapters 6 and 7 is used in the experiments. We attempt to control the first six flexural modes of the beam, so only the first six modes need to be included in our model. The effect of high frequency dynamics is accounted for by adding feedthrough terms in the model.

The models used here are similar to those used in spatial $\mathcal{H}_2$ control in Chapter 7. The transfer function from w and u to the collocated sensor voltage V_s is

$$\hat{G}_{Vs}(s) = \sum_{i=1}^{N} \frac{\Upsilon_i P_i}{s^2 + 2\zeta_i \omega_i s + \omega_i^2} + K_{V_s} \tag{8.11}$$

where $\Upsilon_i = \Omega_1 \Psi_{i1}$ and $P_i = K_1 \Psi_{i1}$.

The transfer function from w and u to the beam transverse deflection y is

$$\hat{G}_r(s,r) = \sum_{i=1}^{N} \frac{\phi_i(r)\, P_i}{s^2 + 2\zeta_i \omega_i s + \omega_i^2} + \sum_{i=N+1}^{N_a} K_{ri}^{opt} \phi_i(r). \tag{8.12}$$

Since we only want to control the first six modes of the beam, we use $N = 6$. Thus, the order of the spatial $\mathcal{H}_\infty$ controller will be 12. From experiments, the feedthrough term in (8.11) is $D_{21} = D_{22} = K_{V_s} = 0.033$. Unlike in Section 7.2, we use the optimal feedthrough term that is based on the spatial $\mathcal{H}_\infty$ approach (4.19):

$$K_{ri}^{opt} = \frac{1}{2}\left(\frac{1}{\omega_i^2} + \frac{1}{\omega_i^2 - \omega_{co}^2}\right) P_i \tag{8.13}$$

where $\omega_{co} \in (\omega_N, \omega_{N+1}) = 795.8$ Hz. The feedthrough term is calculated by considering modes $N+1$ to $N_a = 200$ and assuming that the system damping is small. The spatial $\mathcal{H}_\infty$ case is different from the spatial $\mathcal{H}_2$ case since we do not need to add a second-order term to absorb the feedthrough term into the system dynamics.

The system in (8.1) can be described with

$$A = \begin{bmatrix} 0 & I \\ A_{21} & A_{22} \end{bmatrix}$$

where

$$\begin{aligned} A_{21} &= -\mathrm{diag}(\omega_1^2 \ldots \omega_N^2) \\ A_{22} &= -2\,\mathrm{diag}(\zeta_1\omega_1 \ldots \zeta_N\omega_N) \end{aligned}$$

and

$$\begin{aligned} B_1 &= B_2 = K_1 \begin{bmatrix} 0 & \cdots & 0 & \Psi_{11} & \cdots & \Psi_{N1} \end{bmatrix}^T \\ C_1(r) &= \begin{bmatrix} \phi_1(r) & \cdots & \phi_N(r) & 0 & \cdots & 0 \end{bmatrix} \\ C_2 &= \Omega_1 \begin{bmatrix} \Psi_{11} & \cdots & \Psi_{N1} & 0 & \cdots & 0 \end{bmatrix} \\ D_{11}(r) &= D_{12}(r) = \sum_{i=N+1}^{N_a} K_{ri}^{opt} \phi_i(r) \\ D_{21} &= D_{22} = K_{V_s} = 0.033. \end{aligned} \tag{8.14}$$

The spatial weighting function $Q(r)$ is set equal to one, which means that all points along the beam are weighted equally. Based on (8.8), the performance output $\hat{y}$ in (8.10) is obtained using the orthogonality property of the eigenfunctions and realizing that $D_{11}(r) = D_{12}(r)$:

$$\begin{aligned} \Pi &= \begin{bmatrix} I_{N\times N} & 0_{N\times N} \\ 0_{N\times N} & 0_{N\times N} \\ 0_{1\times N} & 0_{1\times N} \end{bmatrix} \\ \Theta_1 &= \Theta_2 = \begin{bmatrix} 0_{2N\times 1} \\ \left(\sum_{k=N+1}^{N_a} (K_{ri}^{opt})^2\right)^{\frac{1}{2}} \end{bmatrix} \end{aligned} \tag{8.15}$$

where the dimensions of each matrix are described accordingly. The scalar weighting factor R can then be determined to find a controller with sufficient vibration reduction performance and robustness. Matlab μ-Analysis and Synthesis Toolbox was used to calculate our spatial $\mathcal{H}_\infty$ controller based on the system in (8.10). We used $R = 4.78 \times 10^{-7}$ and obtained the solution $\gamma^2 = 9.6 \times 10^{-6}$.

8.3 Experimental implementation

The experimental set-up and apparatus are similar to the those in the two previous chapters (Figure 6.8) whose details can be seen in Chapter 6. The sampling frequency was set at 20 KHz, while the cut-off frequencies at 3 KHz for the two low-pass filters were set at 3 KHz.

Our simulation and experimental results are presented in the following. The frequency response of the controller is shown in Figure 8.2. Similar to the

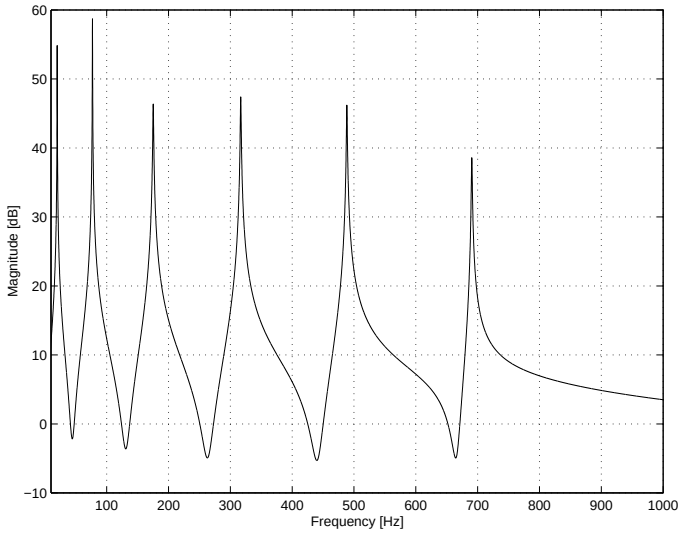

(a) magnitude

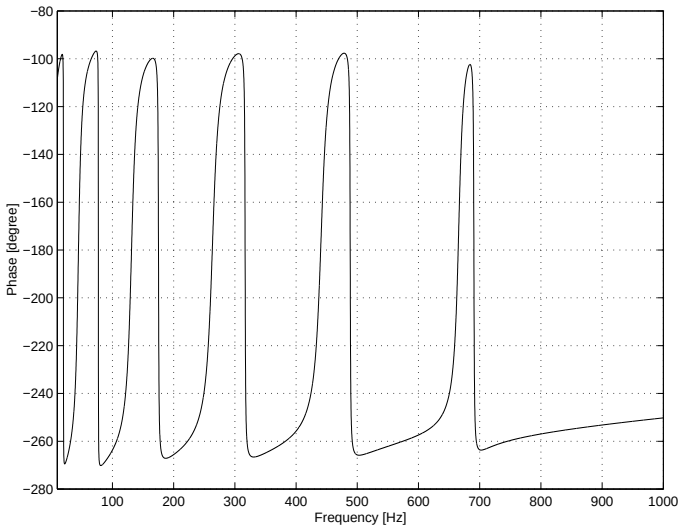

(b) phase

Figure 8.2: The frequency response of the controller (input voltage to output voltage [V/V])

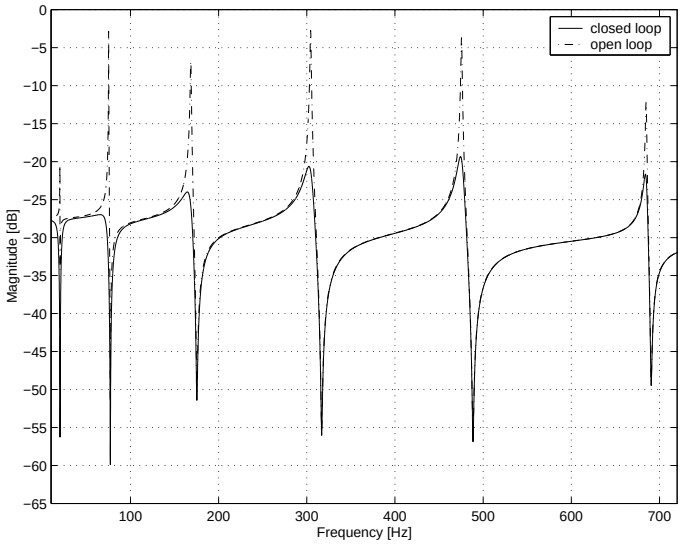

(a) simulation

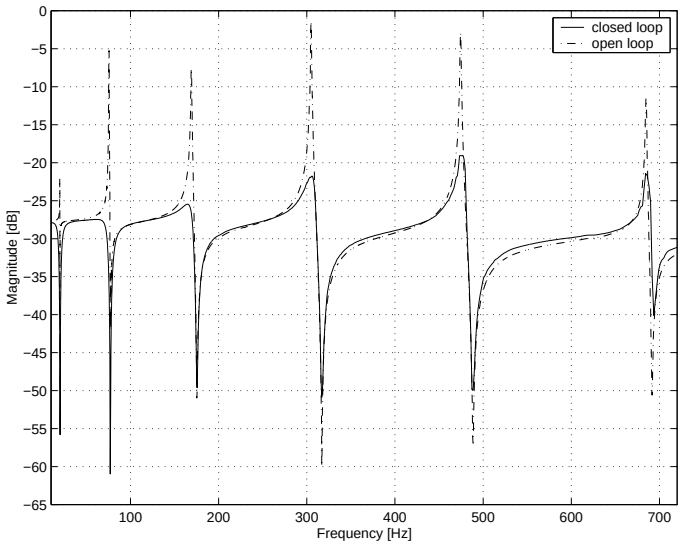

(b) experiment

Figure 8.3: Simulation and experimental frequency responses (actuator voltage to sensor voltage [V/V]) (magnitude)

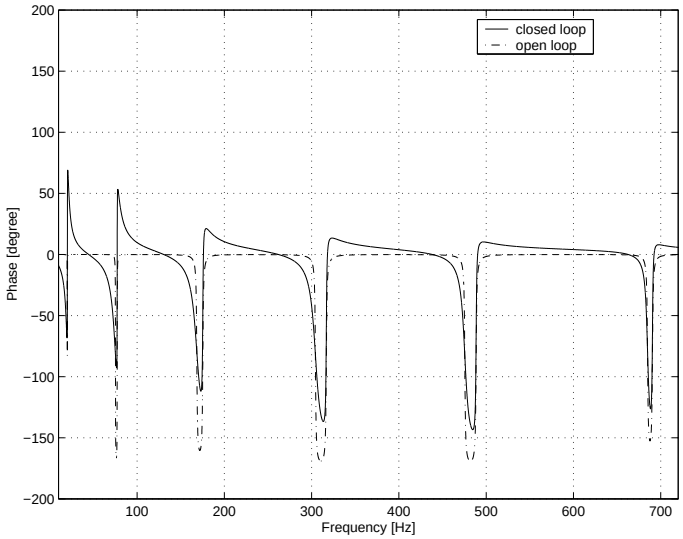

(a) simulation

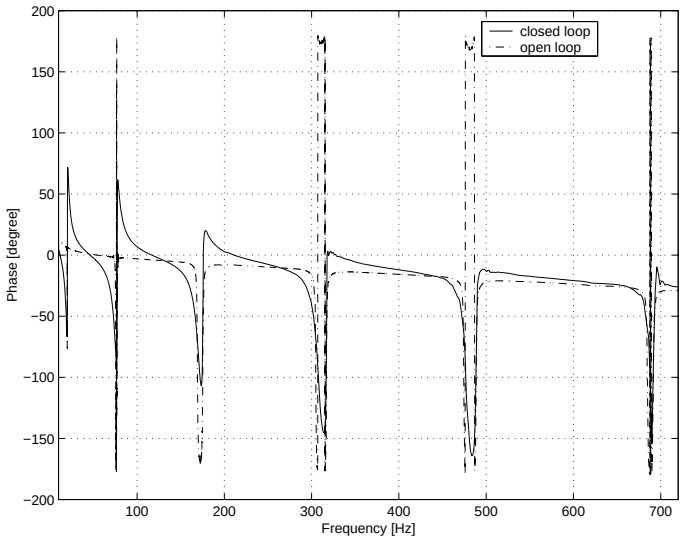

(b) experiment

Figure 8.4: Simulation and experimental frequency responses (actuator voltage to sensor voltage [V/V]) (phase)

two previous chapters, the controller has a resonant nature. Figures 8.3 and 8.4 compare frequency responses of the open-loop and closed-loop systems (actuator voltage to sensor voltage) for both simulation and experimental results. The performance of the controller applied to the real system is as expected from the simulation.

The robustness of the controller can be observed from the loop gain of frequencies up to 1.6 KHz. The plots from simulation and experiment are shown in Figures 8.5 and 8.6 respectively. Our simulation gives a gain margin of 11.3 dB at 1.55 KHz and a phase margin of 89.0^o at 79.3 Hz. The experiment gives a gain margin of 10.7 dB at 1.55 KHz, and a phase margin of 87.1^o at 79.6 Hz. In general, the stability margins predicted by the simulation correspond well with the experiments. Some reduction of the stability margins in the real system is expected because of the phase delay associated with the digital controller and filters used in the experiment as seen in Figure 8.6. Other factors such as model uncertainties may also affect the stability margins.

Figures 8.7 and 8.8 show the simulated spatial frequency responses of the uncontrolled beam and controlled beam respectively. Based on experiments, we can also obtain the spatial frequency responses for the uncontrolled beam and controlled beam shown in Figures 8.9 and 8.10 respectively. The vibration due to the first six modes has been reduced by the spatial $\mathcal{H}_\infty$ controller action. The reduction of resonant responses of modes $1-6$ are approximately $27, 30, 19.5, 19.5, 15.5$ and 8 dB respectively. Thus, our spatial $\mathcal{H}_\infty$ controller minimizes resonant responses of several vibration modes over the entire structure, which is desirable for vibration suppression purposes.

To demonstrate the controller effect on the spatial $\mathcal{H}_\infty$ norm of the system, we plotted the pointwise $\mathcal{H}_\infty$ norm of the controlled and uncontrolled beam as a function of r in Figure 8.11. The experimental and simulation results are reasonably close. It also shows the effect of our spatial $\mathcal{H}_\infty$ controller in reducing the beam vibration. The $\mathcal{H}_\infty$ norm of the entire beam has been reduced by the action of the controller in a more uniform manner spatially. The highest $\mathcal{H}_\infty$

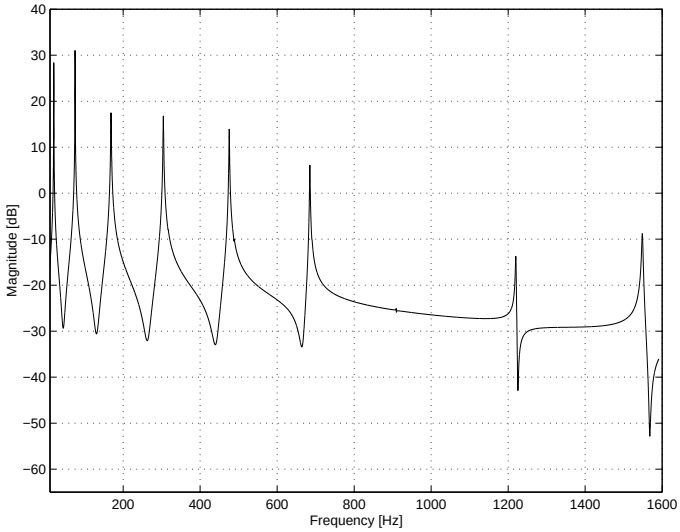

(a) simulation

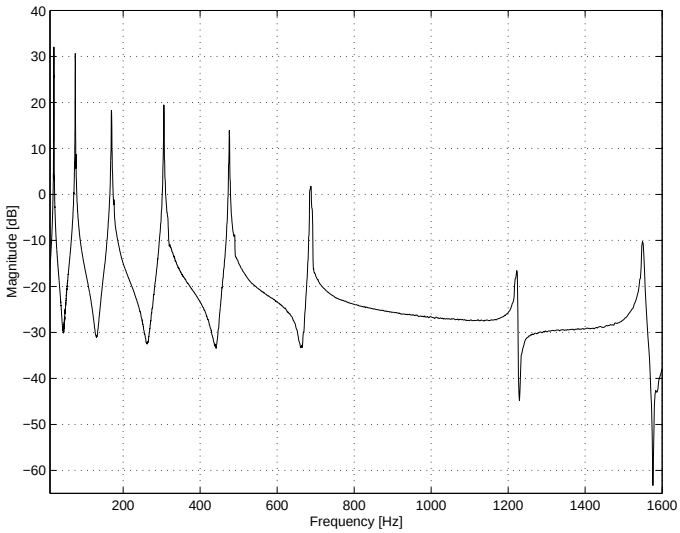

(b) experiment

Figure 8.5: Loop gain [V/V]: simulation and experiment (magnitude)

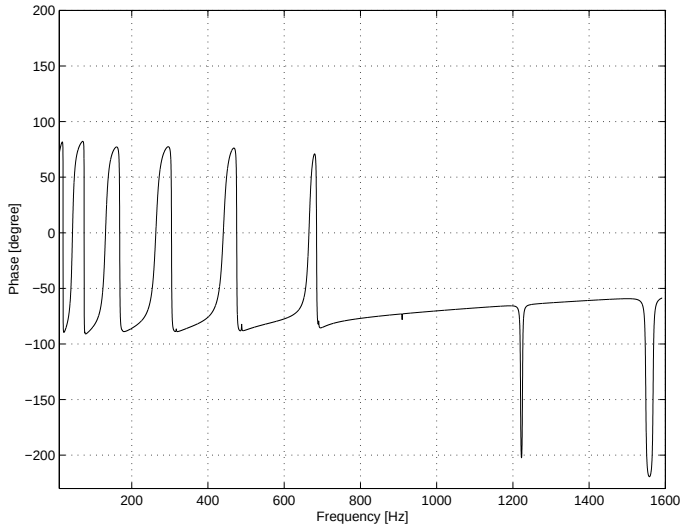

(a) simulation

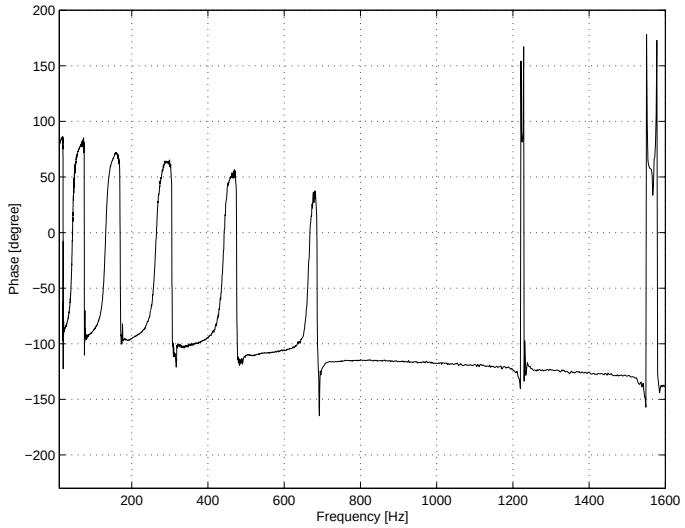

(b) experiment

Figure 8.6: Loop gain [V/V]: simulation and experiment (phase)

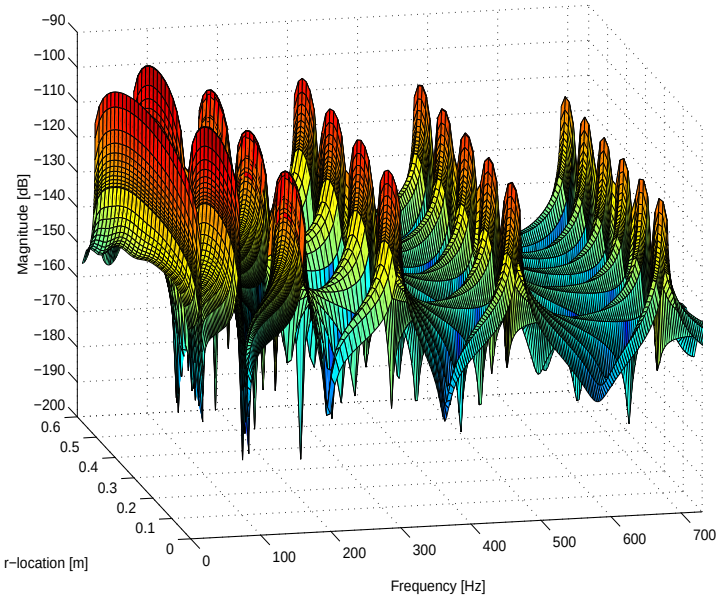

Figure 8.7: The simulated spatial frequency response: actuator voltage to beam deflection [m/V] (open loop)

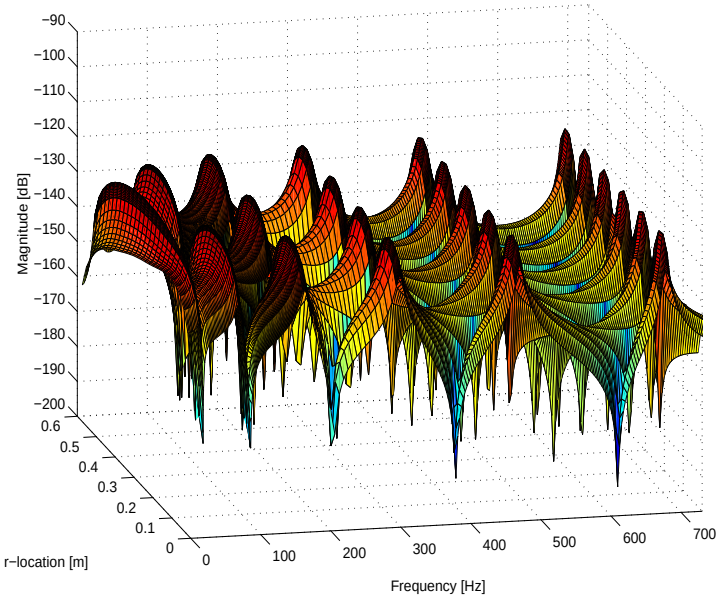

Figure 8.8: The simulated spatial frequency response: actuator voltage to beam deflection [m/V] (closed loop)

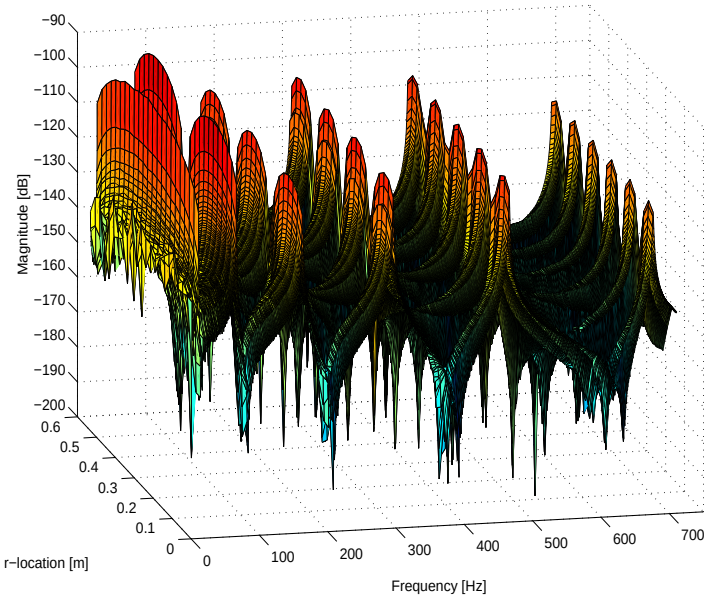

Figure 8.9: The experimental spatial frequency response: actuator voltage to beam deflection [m/V] (open loop)

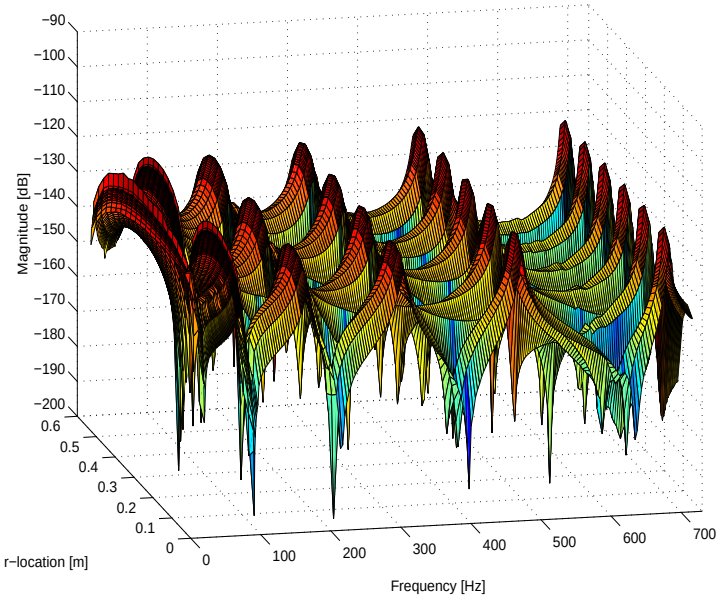

Figure 8.10: The experimental spatial frequency response: actuator voltage to beam deflection [m/V] (closed loop)

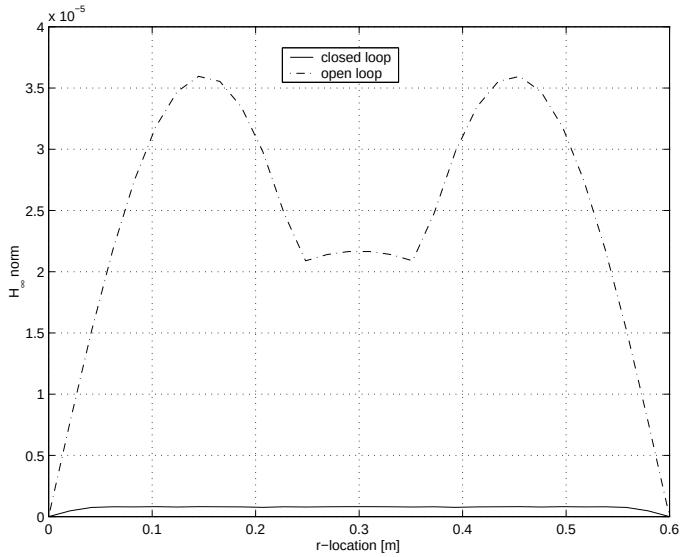

(a) simulation

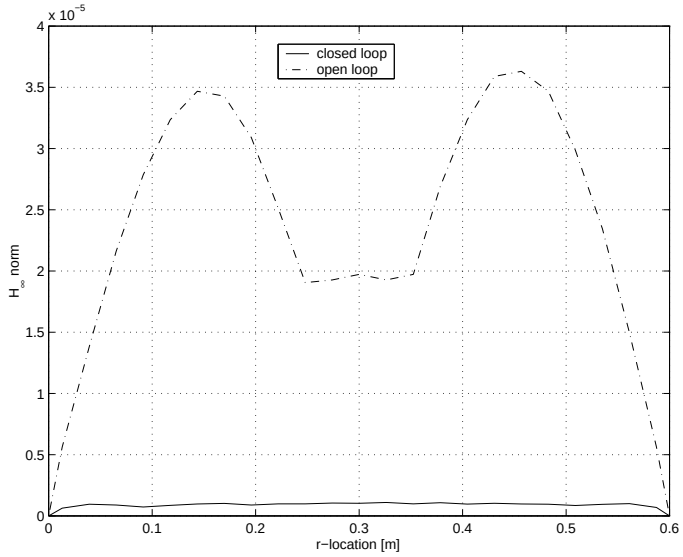

(b) experiment

Figure 8.11: Simulated and experimental $\mathcal{H}_\infty$ norm plots (spatial control)

norm of the uncontrolled beam has been reduced by approximately 97%, from 3.6×10^{-5} to 1.1×10^{-6}.

To demonstrate the effect of the controller in time domain, we performed the following experiments. We applied a pulse signal of 100 V with duration of 15 s through the piezoelectric actuator to simulate an external disturbance. The velocity response of the beam, at a point 80 mm away from one end of the beam, was observed using the PSV Laser Vibrometer. The velocity response was filtered by a band-pass filter from 10 Hz to 750 Hz. The velocity response is shown in Figure 8.12. The settling time of the velocity response has been reduced considerably. The controlled response settled in about 0.5 seconds while the uncontrolled response settled after 8 seconds.

Finally, we want to compare the performance of the spatial $\mathcal{H}_\infty$ control with that of the pointwise $\mathcal{H}_\infty$ control. The following experiment was performed. A pointwise $\mathcal{H}_\infty$ controller was designed to minimize the $\mathcal{H}_\infty$ norm of the transfer function from disturbance w to y at the middle of the beam, i.e. $r = 0.3$ m. The controller had a gain margin of 14.3 dB and a phase margin of 77.9^o and was implemented on the same beam using the set-up in Figure 6.8. Figure 8.13 shows the plot of $\mathcal{H}_\infty$ norm of the controlled and uncontrolled beam as a function of r. The result shows the effectiveness of the pointwise control in local reduction of the $\mathcal{H}_\infty$ norm at and around $r = 0.3$ m. This is not surprising as the only purpose of the controller is to minimize vibration at $r = 0.3$ m. As in the case of pointwise $\mathcal{H}_2$ control, the pointwise $\mathcal{H}_\infty$ controller only suppresses the odd numbered modes since $r = 0.3$ m is a node for even numbered modes.

Comparing Figures 8.11 and 8.13, it can be concluded that the spatial $\mathcal{H}_\infty$ controller has an advantage over the pointwise $\mathcal{H}_\infty$ controller as it minimizes the vibration throughout the entire structure.

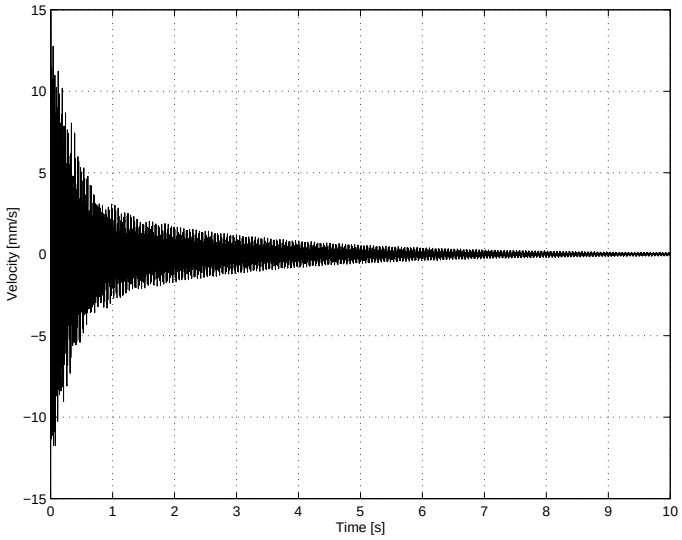

(a) open loop

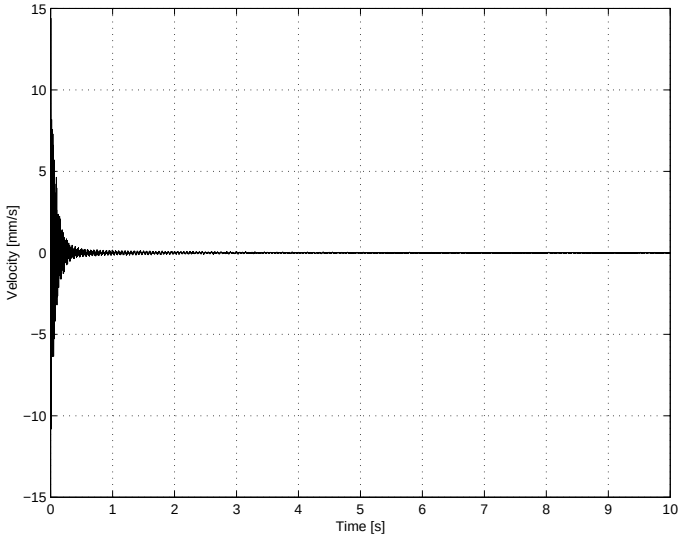

(b) closed loop

Figure 8.12: Vibration at a point 80 mm away from one end of the beam

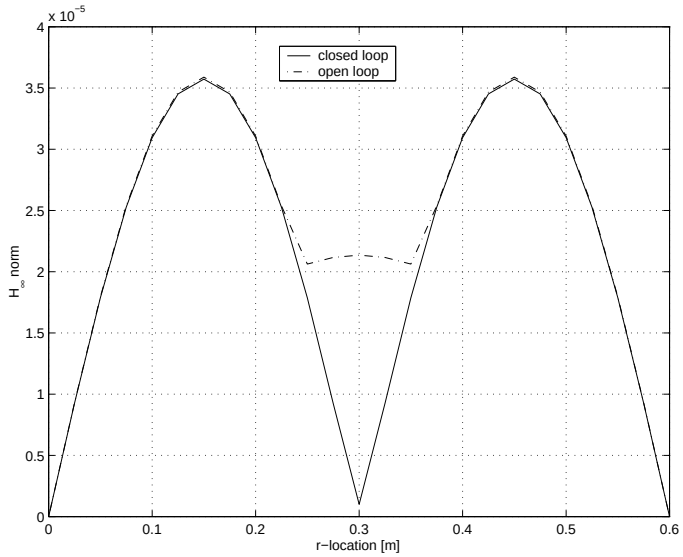

(a) simulation

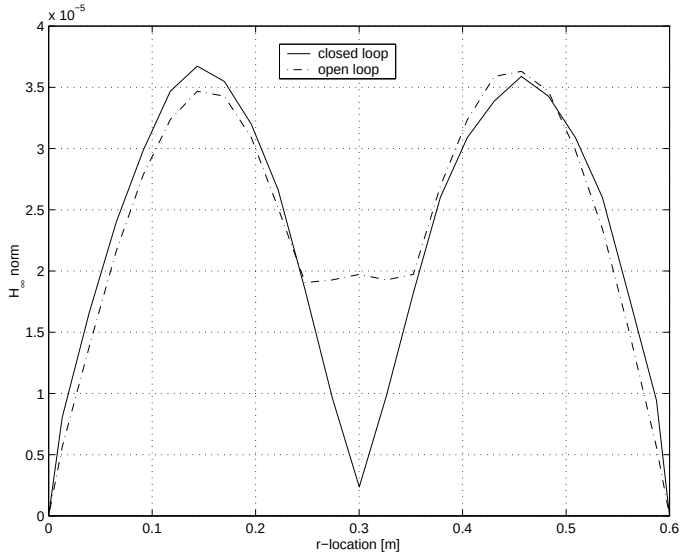

(b) experiment

Figure 8.13: Simulated and experimental $\mathcal{H}_\infty$ norm plots (pointwise control)

8.4 Summary

Based on the concept of the spatial $\mathcal{H}_\infty$ norm, we designed and implemented a spatial $\mathcal{H}_\infty$ controller for vibration control of smart structures. An experimental implementation of the controller was done on a piezoelectric laminate beam. The controller was obtained by solving a standard $\mathcal{H}_\infty$ control problem for a finite-dimensional system. It was observed that such a controller resulted in suppression of vibration of the entire structure by minimizing the spatial $\mathcal{H}_\infty$ norm of the closed-loop system. Experiments demonstrated the effectiveness of the developed controller in reducing structural vibration on a piezoelectric laminate beam. We also showed that the spatial $\mathcal{H}_\infty$ controller has an advantage over the pointwise $\mathcal{H}_\infty$ control in minimizing structural vibration of the entire structure.